Journal of Power Sources 189 (2009) 397–401

Contents lists available at ScienceDirect

Journal of Power Sources

journal homepage: www.elsevier.com/locate/jpowsour

Short communication

Shift of redox potential and kinetics in $Li_x(Mn_yFe_{1-y})PO_4$

Genki Kobayashi [a], Atsuo Yamada [a,*], Shin-ichi Nishimura [a], Ryoji Kanno [a], Yo Kobayashi [b], Shiro Seki [b], Yasutaka Ohno [b], Hajime Miyashiro [b]

[a] Department of Electronic Chemistry, Interdisciplinary Graduate School of Science and Engineering, Tokyo Institute of Technology, 4259 Nagatsuta, Midori, Yokohama 226-8502, Japan
[b] Central Research Institute of Electric Power Industry, 2-11-1 Iwadokita, Komae, Tokyo 201-8511, Japan

ARTICLE INFO

Article history:
Received 19 June 2008
Received in revised form 25 July 2008
Accepted 25 July 2008
Available online 9 August 2008

Keywords:
Olivine
Cathode
Iron
Phosphate
Lithium
Battery

ABSTRACT

The relatively high redox potential in the olivine-type $LiMPO_4$ (M = Mn, Fe, Co, Ni) materials has largely been explained by the M–O–P inductive effect which increases the ionic character of transition metal atoms. Here, we identify the additional perturbative effect that slightly but systematically shifts the redox potential. The substitution of iron by manganese in the olivine $LiMPO_4$ framework raises both of the Fe^{3+}/Fe^{2+} and Mn^{3+}/Mn^{2+} redox potentials by ~0.1 V. The overall volume expansion upon Mn substitution in the whole $Li_x(Mn_yFe_{1-y})PO_4$ system possibly increases the average metal-oxide bond length and hence the ionicity of each transition metal. The voltage shift in a single cell is small but should be significant in a larger-scale battery where there exist a large number of series connections. The kinetic shift for each of the Fe^{3+}/Fe^{2+} and Mn^{3+}/Mn^{2+} redox reactions is also investigated.

1. Introduction

Olivine-type $LiFePO_4$ is now commonly accepted as the most promising cathode material for large-scale lithium batteries [1,2]. The inherent low-cost, non-toxicity, and extremely high stability exhibited by olivine-type $LiFePO_4$, the combination of which conventional cathode materials can never realize, has naturally lead to intensive battery development toward large-scale applications such as plug-in hybrid vehicles.

The high M^{3+}/M^{2+} redox potential generated by the electrochemical reaction in Li_xMPO_4 (Fe: 3.4 V; Mn: 4.1 V; Co: 4.8 V; Ni: 5.1 V) has previously been discussed in terms of the local M–O–P linkage in the olivine structure, which induces a super exchange interaction called 'inductive effect' [1–5]. The strongly covalent P–O bond in PO_4^{3-} makes the neighboring transition metal atoms strongly ionic, stabilizing the antibonding state that is primarily Fe 3d in character and "tunes" the M^{3+}/M^{2+} redox energy to a useful level. In fact, modification of the electronic structure by this effect is large enough to exceed 1 eV, as the Fe^{3+}/Fe^{2+} redox potential in the simple iron oxide is lower than 2 V vs. Li/Li^+.

In this short report, an additional perturbative modification of the redox potential and changes in the polarization of the redox couples are investigated and these systematic static/kinetic effects will be discussed in terms of the overall change in lattice dimensions.

2. Experimental

Pure, single-phase $Li(Mn_yFe_{1-y})PO_4$ (y = 0, 0.2, 0.4, 0.6, 0.8, 1.0) powders were synthesized using a solid-state reaction. A stoichiometric amount of lithium carbonate [Li_2CO_3, Wako, >99%], iron(II) oxalate dihydrate [$FeC_2O_4{\cdot}2H_2O$, JUNSEI, 99%], manganese(II) oxalate hemihydrates [$MnC_2O_4{\cdot}0.5H_2O$, Wako, >99%], and diammonium hydrogen phosphate [$(NH_4)_2HPO_4$, Wako, >99%] were used as starting materials. To provide the electronic conductivity in the final electrode composite, porous Ketjen Black (Lion, ECP, 10 wt.% as final content in the electrode composite) was included. A total 5 g of raw materials was poured into a 250-mL Cr-hardened SUS container with Cr-hardened SUS balls (10 mmf × 10 and 5 mmf × 16) and thoroughly mixed by a conventional planetary milling apparatus (ITOH $LAPO_4$) for 24 h. The olivine phase was synthesized by sintering at 600 °C for 6 h in a purified Ar gas flow.

Electrochemical measurements were performed using 2032-type coin cells with VMP2/Z (Princeton Applied Research) at 30 °C. The working electrode was a ratio of 85:10:5 (w/w) cathode

* Corresponding author. Tel.: +81 45 924 5403; fax: +81 45 924 5403.
E-mail address: yamada@echem.titech.ac.jp (A. Yamada).

0378-7753/$ – see front matter © 2008 Elsevier B.V. All rights reserved.
doi:10.1016/j.jpowsour.2008.07.085

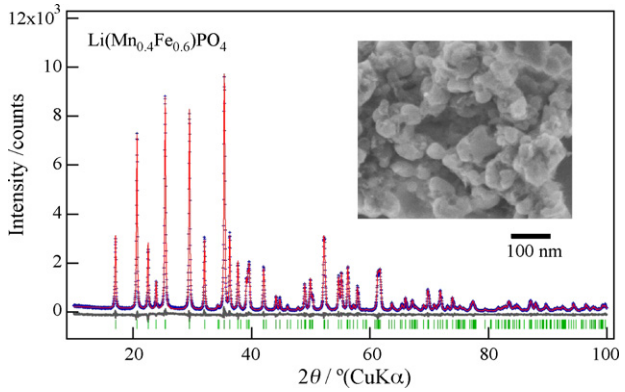

Fig. 1. Rietveld refinement pattern of the X-ray data for $Li(Mn_{0.4}Fe_{0.6})PO_4$ at room temperature.

composite, conductive carbon (acetylene black), and polytetrafluoroethylene, respectively. The electrolyte was a 1-M solution of $LiPF_6$ in 1:1 ethylene carbonate/dimethylcarbonate (EC/DMC) and the counter electrode was a disc type lithium metal foil. The open-circuit voltage (OCV) measurements were performed starting from the fully discharged state and moving in the anodic direction, with intermittent of 2.5% state of charge (SOC). The full discharge was realized by setting the cell voltage to 2.5 V for 24 h after discharging the cell galvanostatically at C/20 rate. The charging rate was set to C/20, followed by the 24 h of relaxation for equilibrium at each measuring points. The OCV measurements were also performed starting from fully charged state toward cathodic direction with identical relaxation condition to confirm the measured OCV include negligible kinetic effect. For cyclic voltammetry measurements, a repeated liner potential sweep mode was applied with a scan rate of $10\,mV\,s^{-1}$ in the range of 3.0–4.8 V vs. Li/Li^+.

Powder diffraction patterns were measured with an X-ray diffractometer (Rigaku, RINT TTR-III) using Cu Kα radiation. Structural parameters were refined by Rietveld analysis using TOPAS software (version 3). For samples with lithium compositions of $x=y$ in $Li_x(Mn_yFe_{1-y})PO_4$, Hosen type cells (HS test cell, Hosen Co.) were assembled and set to 3.8 V vs. Li/Li^+ with an equilibrium condition of <100 nA. The cells were then dismantled in an Ar glove box and the cathodes were washed with dimethyl carbonate (DMC), before being subjected to ex situ diffraction measurements using a tightly sealed sample holder filled with Ar.

3. Results and discussions

The X-ray diffraction profiles for pristine $Li(Mn_yFe_{1-y})PO_4/C$ ($y=0$, 0.2, 0.4, 0.6, 0.8, 1.0) were refined with orthorhombic *Pnma*. No impurities were identified. Fig. 1 and Table 1 show the Rietveld refinement results and SEM picture of $Li(Mn_{0.4}Fe_{0.6})PO_4$ as a typical example. The crystalline size of a series of $Li(Mn_yFe_{1-y})PO_4$ compounds estimated by the two methods (SEM and coherent length by XRD) was consistent, almost identical and estimated to be ~80 nm. Using these pure samples with almost identical particle size and particle morphology, the electrochemical properties of $Li(Mn_yFe_{1-y})PO_4$ were investigated.

A large reversible capacity of 160–170 $mAh\,g^{-1}$ was confirmed for all samples, and is close to the theoretical capacity. Fig. 2 shows the OCV curves measured for a series of $Li(Mn_yFe_{1-y})PO_4$ ($y=0$, 0.2, 0.4, 0.6, 0.8, 1.0). The capacity ratio for the regions at ~4.1 V (Mn^{3+}/Mn^{2+}) and at ~3.4 V (Fe^{3+}/Fe^{2+}) is the same as the initial manganese/iron ratio (Fig. 2(a)). Clearly, the redox potentials for both Fe^{3+}/Fe^{2+} (Fig. 2(b)) and Mn^{3+}/Mn^{2+} (Fig. 2(c)) are progressively increased as a function of the initial manganese content y, until the shift finally approaches 0.1 V. Such an up-shift of the redox potential was observed both for cathodic/anodic experiments with identical equilibrium condition. The slopy region around $x=y$ has been attributed to the lithium compositional domain with solid-solution reaction [3].

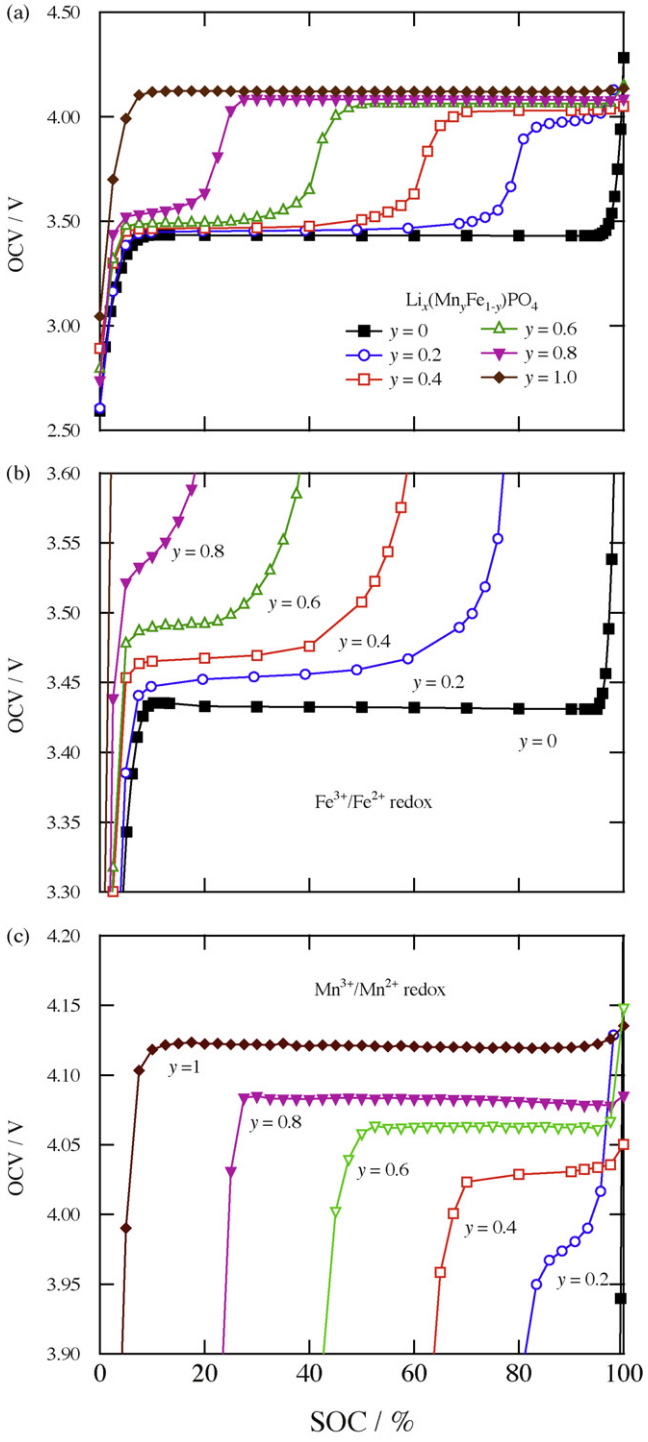

Fig. 2. (a) A comparison of open-circuit voltage curves at 30 °C with a different initial Mn content y. (b) Expanded view of the Fe^{3+}/Fe^{2+} redox region ($x<y$). (c) Expanded view of the Mn^{3+}/Mn^{2+} redox region ($x>y$).

Table 1
Rietveld refinement results for $Li(Mn_{0.4}Fe_{0.6})PO_4$ with X-ray diffraction data

Atom	Site	g	x	y	z	B (Å^2)
Li	4a	1	0	0	0	1
Fe, Mn	4c	1	0.28202 (6)	0.25	0.97369 (18)	0.6
P	4c	1	0.09406 (13)	0.25	0.4120 (3)	0.6
O_1	4c	1	0.09734 (3)	0.25	0.7417 (5)	1
O_2	4c	1	0.4536 (4)	0.25	0.2105 (5)	1
O_3	8d	1	0.1653 (2)	0.0449 (3)	0.2783 (4)	1

$a = 10.37744\ (14)$ Å, $b = 6.04445\ (9)$ Å, $c = 4.71473\ (7)$ Å, $R_{exp} = 5.15\%$, $R_{wp} = 6.99\%$, $R_p = 4.93\%$, GOF $= R_{wp}/R_{exp} = 1.36$, $R_B = 1.818\%$

Such highly systematic shifts in OCV plateaus were also confirmed by CV measurements (Fig. 3a). An increase in Mn/Fe ratio leads to the shift of the midpoint of cathodic and anodic current peaks toward higher potential for both the Fe^{3+}/Fe^{2+} and Mn^{3+}/Mn^{2+} redox couples (Fig. 3b), where the overall shift range is ~0.1 V, which is consistent with the potential shift observed in OCV curves in Fig. 2.

Further noticeable changes in the CV profiles can be found in the anodic/cathodic peak separation as well as in the peak widths (Fig. 3a and c) and, unlike the shift of equilibrium potential demonstrated in the preceding sections, are related to a kinetic issue. The magnitude of peak separation shows an opposite tendency for the Mn^{3+}/Mn^{2+} and Fe^{3+}/Fe^{2+} couples, the former abruptly widening (0.065–0.379 V) while the latter narrows slightly (0.116–0.06 V). A similar trend can be seen in the peak widths; for Fe^{3+}/Fe^{2+} the peak widths are almost unchanged whereas broadening of the Mn^{3+}/Mn^{2+} peaks is evident. The abrupt loss of redox activity of Mn^{3+}/Mn^{2+} upon increasing manganese content is a well-known fact [6,7] that has been discussed from various points of view including structural instability in the Mn^{3+} phase [6], smaller intrinsic electronic/ionic conductivities [7,8], larger lattice mismatching in two-phase reactions [7,9], and the energy difference between surface and bulk states [10]. However, the experiments reported here have shown that the kinetics of Fe^{3+}/Fe^{2+} redox couple in the $Li_x(Mn_yFe_{1-y})PO_4$ exhibit independent and opposite behavior as a function of Mn content y. This implies that activities of the two redox couples is not a simple function of the transport properties in

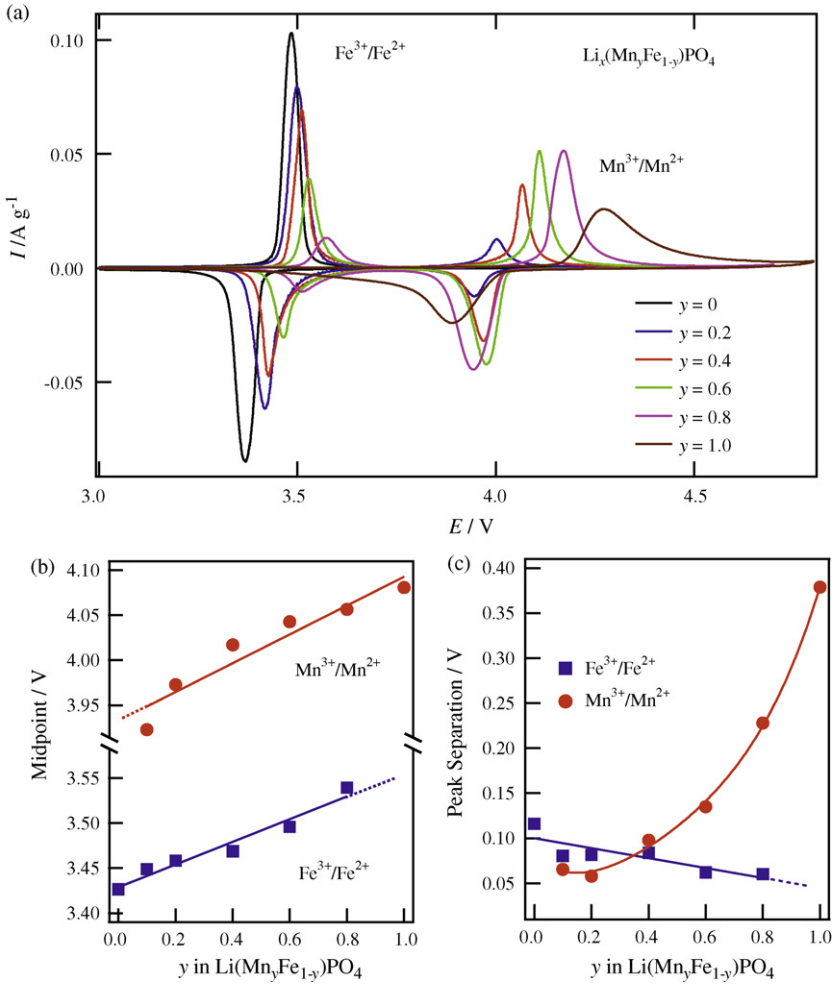

Fig. 3. (a) CV profiles of $Li(Mn_yFe_{1-y})PO_4$ with different Mn content y. (b) The shift of the midpoint of cathodic and anodic peaks for each Fe^{3+}/Fe^{2+} and Mn^{3+}/Mn^{2+} redox couples as a function of the Mn content y. (c) Change in the magnitude of peak separation for Fe^{3+}/Fe^{2+} and Mn^{3+}/Mn^{2+} as a function of the Mn content y.

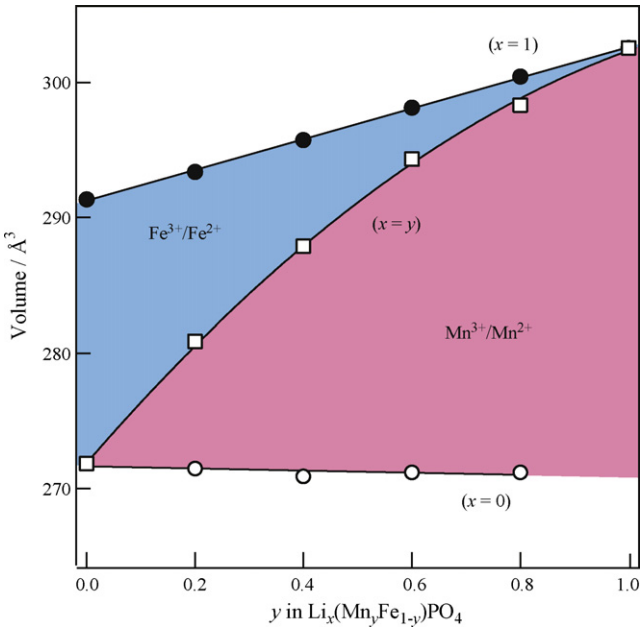

Fig. 4. Change in the unit cell volume as a function of Mn content y in $Li(Mn_y^{2+}Fe_{1-y}^{2+})PO_4$ (discharge state, $x=1$), $(Mn_y^{3+}Fe_{1-y}^{3+})PO_4$ (charge state, $x=0$), and $Li_x(Mn_y^{2+}Fe_{1-y}^{3+})PO_4$ (intermediate sate, $x=y$). The blue and red regions correspond to the Fe^{3+}/Fe^{2+} and Mn^{3+}/Mn^{2+} redox reactions.

the end members ($x=0$, 1) and may give some hints towards understanding the whole reaction mechanism of the olivine-type Li_xMPO_4.

One possible explanation for the manganese-induced potential up-shift and the opposite kinetic behavior of Mn^{3+}/Mn^{2+} and Fe^{3+}/Fe^{2+} redox reactions lies in the overall volume expansion in the whole (x, y) compositional region of $Li_x(Mn_yFe_{1-y})PO_4$. The unit cell volume refined for the three series of samples, $x=1$, $x=0$, and $x=y$, are summarized in Fig. 4 as a function of Mn content y. Here the intermediate $x=y$ samples are defined as equilibrium states at 3.8 V vs. Li/Li^+, given the OCV curves in Fig. 2. A simple isotropic lattice expansion was confirmed for a series of $Li(Mn_y^{2+}Fe_{1-y}^{2+})PO_4$ compounds (discharged state, $x=1$), whereas the $(Mn_y^{3+}Fe_{1-y}^{3+})PO_4$ series (charged state) showed constant volume, consistent with the previous literature [6,11]. This is due to the differences in the ionic radii in the high-spin state; Mn^{2+} (0.97 Å) > Fe^{2+} (0.92 Å), and Mn^{3+} (0.79 Å) = Fe^{3+} (0.79 Å). The unit cell dimensions of the intermediate state at $x=y$ in $Li_x(Mn_y^{2+}Fe_{1-y}^{3+})PO_4$ were refined and the resulting lattice volumes are plotted in Fig. 4, where Mn^{3+}/Mn^{2+} occurs at $x<y$ and Fe^{3+}/Fe^{2+} occurs at $x>y$. An important point to note is that all phases included in the redox reaction in $Li_x(Mn_yFe_{1-y})PO_4$ show volume expansion with increase of Mn content. These observations include both the effects of the change in ionic radius and of the lithium content. As the PO_4 polyanion in the $LiMPO_4$ structure is very rigid, a major contribution to such volume expansion is known to be the elongation of M–O bond lengths [11] which has the effect of enhancing the ionic character of the transition metals. This situation can lower the Fe 3d–O 2p antibonding state leading to the higher redox potential.

The concept of the inductive effect has already been established in various lithium intercalation polyanion compounds. It induces large potential up-shift of a redox reaction, typically by more than 1 V. Difference in the geometric polyhedral network has also been known to give additional potential shift [12]. However, the final essential feature is the extent of covalency or ionicity of the bonding between the redox center and oxygen. In our present case for $Li_x(Mn_yFe_{1-y})PO_4$, the covalency or ionicity of the (Mn, Fe)–O bond is adjusted by the lattice dimensions and hence by the local (Mn, Fe)–O bond lengths under the identical crystal structure. Clearly, this simple modification is effective enough to shift the redox potential by ~0.1 V. While the shift of 0.1 V is slight for a single cell, in a large-scale battery such as for electric vehicles, a large number of cells are connected in series. This would result in an accumulation of the slight voltage shift.

Meethong et al. [9,13] have recently pointed out the importance of strain accommodation at the two-phase interface, indicating that a smaller mismatch is advantageous to form a continuous "coherent" interface. The "coherent" interface was claimed to be suitable for a facile cooperative movement of the phase boundary, because "incoherency" would be accompanied by a movement of heavy ions such as P, Fe, leading to a formation of more serious macroscopic dislocations or cracks. From this viewpoint, the implications of Fig. 4 include a reduced mismatch in the Fe^{3+}/Fe^{2+} redox reaction (blue region) and, conversely, an increased mismatch in the Mn^{3+}/Mn^{2+} redox reaction (red region) as a function of the Mn content. These opposing tendencies in variations of lattice mismatch are consistent with the observed change in the polarization of the Fe^{3+}/Fe^{2+} (reduced) and Mn^{3+}/Mn^{2+} (increased) redox couples, and may, at least in part, give an additional insights into the previous kinetic discussions on this system based on the bulk/surface transport properties and structural stability.

4. Conclusion

The careful electrochemical experiments on $Li_x(Mn_yFe_{1-y})PO_4$ have led to the two hitherto unidentified unique features in this system: (i) a systematic up-shift of the redox potential for both Fe^{3+}/Fe^{2+} and Mn^{3+}/Mn^{2+} by 0.1 V; (ii) an opposite kinetic effect, reduced polarization in the Fe^{3+}/Fe^{2+} plateau while increased polarization in the Mn^{3+}/Mn^{2+} plateau upon increasing Mn content. These highly systematic equilibrium/kinetic effects were explained in terms of the slight modifications of the (Mn, Fe)–O bond character and coherent interfacial model for phase boundary movement, contributing to a more comprehensive understanding of the electrode reaction in olivine-type materials. The practical impacts of the potential shift are unknown but may be influential in a large-scale battery with a large number of series connections.

Acknowledgements

This work was financially supported by the Ministry of Education, Culture, Sports, Science and Technology of Japan, through a Grant-in-Aid for Scientific Research (A) No. 19205027, and the New Energy and Industrial Technology Development Organization (NEDO) through the research grant to A.Y.

References

[1] A.K. Padhi, K.S. Nanjundaswamy, J.B. Goodenough, J. Electrochem. Soc. 144 (1997) 1188.
[2] A. Yamada, S.C. Chung, K. Hinokuma, J. Electrochem. Soc. 148 (2001) A224.
[3] A. Yamada, Y. Kudo, K.Y. Liu, J. Electrochem. Soc. 148 (2001) A747.
[4] K. Amine, H. Yasuda, M. Yamachi, Electrochem. Solid-State Lett,. 3 (2000) 178.
[5] J. Wolfenstine, J. Allen, J. Power Sources 142 (2005) 389.
[6] A. Yamada, S.C. Chung, J. Electrochem. Soc. 148 (2001) A960.
[7] M. Yonemura, A. Yamada, Y. Takei, N. Sonoyama, R. Kanno, J. Electcochem. Soc. 151 (2004) A1352.
[8] C. Delacourt, L. Laffont, R. Bouchet, C. Wurm, J.-B. Leriche, M. Morcrette, J.-M. Tarascon, C. Masquelier, J. Electrochem. Soc. 152 (2005) A913.

[9] N. Meethong, H.Y. Huang, S.A. Speakman, W.C. Carter, Y.M. Chiang, Adv. Funct. Mater. 17 (2007) 1115.
[10] L. Wang, F. Zhou, G. Ceder, Electrochem. Solid-State Lett. 11 (2008) A94.
[11] A. Yamada, Y. Takei, H. Koizumi, N. Sonoyama, R. Kanno, K. Itoh, M. Yonemura, T. Kamiyama, Chem. Mater. 18 (2006) 804.
[12] A.K. Padhi, K.S. Nanjundaswamy, C. Masquelier, S. Okada, J.B. Goodenough, J. Electrochem. Soc. 144 (1997) 1609.
[13] N. Meethong, H.Y. Huang, W.C. Carter, Y.M. Chiang, Electrochem. Solid-State Lett. 10 (2007) A134.